Assessment of qualitative and quantitative features in coronary artery MRA

Jérôme Velut, Pierre-Axel Lentz, Dominique Boulmier, Jean-Louis Coatrieux,
Christine Toumoulin

▶ **To cite this version:**

Assessment of qualitative and quantitative features in coronary artery MRA
Évaluation de caractéristiques qualitatives et quantitatives en angiographie IRM des artères coronaires

Jérôme Velut[a,b], Pierre-Axel Lentz[c], Dominique Boulmier[c], Jean-Louis Coatrieux[a,b], Christine Toumoulin[a,b]

[a]*LTSI, Université de Rennes 1, Campus de Beaulieu, Bât 22, Rennes, F-35042 Cedex*
[b]*INSERM, U642, Rennes, F-35000, France*
[c]*CHU Pontchaillou, Service de Radiologie, Rennes, F-35000*

Abstract

In this paper, an analysis of the coronary trees using Magnetic Resonance Angiography (MRA) is performed. The objective is to estimate how much MRA is capable to provide insights into the vascular network. A qualitative exploration of the MRA volumes with anatomical labelling by experts is first performed, Quantitative vessel features are then manually extracted providing a ground truth which is further compared to a semi-automatic extraction. This evaluation is carried out on 10 datasets of the SSFP MRA sequence and allows getting a more precise view on the current state-of-the-art as well as on future achievements to be done.

Résumé

Nous proposons une analyse des artères coronaires en angiographie IRM. L'objectif est d'estimer la profondeur à laquelle l'angio-IRM peut conduire dans un réseau vasculaire coronaire. Une exploration qualitative est décrite

en premier lieu. Une quantification de certaines caractéristiques des vaisseaux sont extraites manuellement, pour servir de vérité de terrain dans le cadre d'une évaluation préliminaire d'une méthode d'extraction semi-automatique. Cette évaluation, qui porte sur 10 volumes de cœur entier obtenus partir de la séquence SSFP, apporte un éclaircissement sur l'état de l'art ainsi que sur les progrès envisageables.

1. Introduction

According to the recent heart disease and stroke statistics update, "death rates from cardiovascular disease (CVD) have declined, yet the burden of disease remains high" [1]. Efforts made until now have proven profitable for western countries, where CVD are known as the leading cause of death. However, an earlier and better diagnostic of coronary artery diseases (CAD) based on the advances made in imaging modalities leads to a significant decrease of mortality [2, 3]. Moreover, new therapies that rely on cardiac veins extraction, like biventricular pacing, known as cardiac resynchronization therapy (CRT), open also new perspectives for patient care [4]. In both cases, imaging sources play an important role as it enables to detect and characterize potential pathological patterns and to elaborate sound planning for therapy and efficient patient followup [5]. They provide relevant anatomical knowledge of the human heart vasculatures (either morphometric [6, 7], structural [8, 9] or both [10]) which can be confronted to patient-specific data in a therapeutic or surgical decisional process. Despite the high resolution of the

2

X-Ray angiography, the gold standard for coronary analysis, and the many attempts in reconstruction from few views [11, 12, 13], other techniques are increasingly being used in clinical protocols : Multidetector Computed Tomography (MDCT), Electron Beam Computed Tomography (EBCT) and Magnetic Resonance Angiography (MRA) [14, 15].

MRA is of interest for several reasons : (1) no ionizing radiation is used, (2) improved assessment of aneurysms and CAD are expected, and (3) MR imaging provides acquisition sequences that allow focusing on different anatomical or physiological characteristics. Recent works show that MRA could discriminate significant ($> 50\%$) from non-significant stenosis [16] and is a reliable imaging method for anatomy assessment before a surgical intervention [17]. However, they do not report yet precise quantitative features. The state-of-art of MR sequences used for clinical studies are those based on steady-state free precession (SSFP) technique [18, 19]. Whole-heart acquisition makes the image analysis less operator dependent by including the vessels up to distal vascular parts in a single volume. Used in conjonction with navigators, it is possible to image a whole heart without β—blockers, without contrast agent and in a free-breathing fashion. These points are of importance when diagnostic is performed on symptomatic patients.

A meta-analysis of CAD diagnostic performance of coronary MRA [20] reports a moderately high sensitivity for detecting proximal stenoses but notes that distal segments can not be evaluated. The clinical study conducted in [21] on congenital heart disease diagnostic based on SSFP MR Imaging focuses therefore on proximal segments.

This paper is aimed at answering two questions : (1) what can be expected

in terms of visual exploration and manual extraction of vascular structures by expert ? (2) what difficulties and performance can be anticipated for semi-automatic quantitation ?

10 whole-heart coronary artery SSFP MRA have been studied. The datasets are first described (2) and then qualitatively analysed (Section 3.2). Furthermore, a quantitative study, expert-based, is carried out in order to assess patient and inter-patient the variability of different features (Section 3.3). A preliminary comparison of the manual extractions with an existing semi-automatic centreline tracking algorithm is then presented in Section 4 and allows concluding on factual benefits and future challenge of whole-heart coronary artery imaging.

2. Technical and anatomical background

2.1. Datasets

The 10 datasets were acquired on a 1.5T system (Philips Intera and Achieva) using a steady-state free precession (SSFP) MR sequence [18], at end-diastolic phase without contrast agent. The MR sequence parameters are summarized in table 1. Table 2 shows different characteristics of the MRA volumes. The field of view corresponds to the whole acquired volume, while the VOI is the volume of the bounding box comprising the visible coronary vasculature. The intensity range is measured inside the VOI. All the volume have the same in-plane resolution, being 512×512 isotropic pixels of size $0.59\ mm$ whereas the interslice distance and the number of slices vary.

4

Parameters	
TR	$4.04 - 4.75ms$
TE	$2.01 - 2.38ms$
Flip angle	$70.00 - 90.00$
Pixel size	$0.5 - 0.7mm$
Matrix size	512×512
Slice distance	$0.7 - 0.9mm$
Number of slices	$100 - 170$

TAB. 1: MR sequence parameters

Volume	Slices distance (mm)	Number of slices	Field of view (cm^3)	VOI (cm^3)	Intensity range
1	0.85	159	12163.5	761.3	$0 - 673$
2	0.9	109	8829	721.5	$0 - 740$
3	0.8	149	10728	828.5	$0 - 627$
4	0.85	139	10633.5	542.8	$0 - 949$
5	0.8	139	10008	790.8	$0 - 588$
6	0.85	139	10633.5	724.1	$0 - 671$
7	0.75	169	11407.5	789.2	$0 - 611$
8	0.85	129	9868.5	478.6	$0 - 560$
9	0.85	139	10633.5	880.1	$0 - 542$
10	0.85	139	10633.5	353.3	$0 - 1054$

TAB. 2: Volume characteristics

Segment	Map location	Acronym
1	Proximal right coronary artery conduit segment	RCA(p)
2	Mid-right coronary artery conduit segment	RCA(m)
3	Distal-right coronary artery conduit segment	RCA(d)
4	Right posterior descending artery segment	RPD
5	Right posterior atrioventricular segment	RPA
6	First right posterolateral segment	RPL(1)
7	Second right posterolateral segment	RPL(2)
8	Third right posterolateral segment	RPL(3)
9	Posterior descending septal perforators segment	PDS
10	Acute marginal segment(s)	RCA-AM

TAB. 3: Right coronary artery map correspondence.

2.2. Anatomical considerations

In the following and for the whole paper, anatomical nomenclature is based on the classification established by the American Heart Association [22]. Figure 1 shows the anatomical segments and their corresponding names depicted in tables 3 and 4. For clarity purpose, and because some distal segments have never been evaluated in the litterature, we propose reader-friendly acronyms in the remaining of the paper.

3. Labelization and manual extraction

Existing studies, even recent, on whole-heart coronary MRA lack of in-depth qualitative and quantitative analysis. In this section, we present the result of the manual extraction of the coronary arterial trees from the 10 datasets. The anatomical nomenclature and the labelling performed in colla-

Segment	Map location	Acronym
11	Left main coronary artery segment	LM
12	Proximal LAD artery segment	LAD(p)
13	Mid-LAD artery segment	LAD(m)
14	Distal LAD artery segment	LAD(d)
15(a)	(Lateral) first diagonal branch segment	DIAG(1)
16(a)	(Lateral) second diagonal branch segment	DIAG(2)
17	LAD septal perforator segments	LASP
18	Proximal circumflex artery segment	CX(p)
19(a)	Mid (distal)-circumflex artery segment	CX(md)
20(a)	(Lateral) first obtuse marginal branch segment	OBTM(1)
21(a)	(Lateral) second obtuse marginal branch segment	OBTM(2)
22(a)	(Lateral) third obtuse marginal branch segment	OBTM(3)
23	Circumflex artery AV groove continuation segment	CX(g)
24	First left posterolateral branch segment	LPL(1)
25	Second left posterolateral branch segment	LPL(2)
26	Third left posterolateral branch segment	LPL(3)
27	Left posterolateral descending artery segment	LPD
28(a)	(Lateral) ramus intermedius segment	RIS
29(a)	(Lateral) third diagonal branch segment	DIAG(3)

TAB. 4: Left coronary artery map correspondence.

boration with a radiologist and a cardiologist are confronted. Finally, some basic vessel features (length, diameter and image intensity) are quantified and results discussed.

3.1. Coronary arterial trees extraction procedure

3.1.1. Rough manual centreline extraction

The manual extractions have been performed by interactively pointing inside the vessels on the axial slices of the volumes. The resulting curves having a non-uniform sampling, a slight smoothing was applied based on a decimation/refinement procedure.

Decimation The manually-extracted curves are evenly resampled along a cardinal spline interpolating the initial point set. Sampling step is 3 mm long.

Refining The decimated curve is then resampled along a cardinal spline but with a 1 mm sampling step.

Figure 2 shows the ten arterial trees obtained from this interactive procedure. By slicing the MR dataset orthogonally to the curves, it is possible to carry out a straightened reformation of the arteries. A volume rendering of such a reformation is depicted in figure 3. This view is based on the Straightened Curved Planar Reformation (Sa-CPR) described in [23].

3.1.2. Centreline correction

A centreline correction, similar to the one presented in [24], is performed to ensure an accurate localization of the vessel centre. The main drawback of an axial-exclusive slice pointing is that the center of a vessel is not reliably located when the vessel runs tangentially to the axial plane. It may lead to an

inaccurate location of the centreline for a non-negligible length of coronary arteries (eg RCA 3rd segment, posterio- and atrio-ventricular segments). To deal with this issue, the consideration that slicing axially the Sa-CPR is equivalent to slicing orthogonally along the vessel allows us to point trustfully the center of the vessel at each Sa-CPR axial slice. A corrected centerline is then produced, as shown in figure 4.

3.1.3. Radius estimation

This corrected centreline is used as a reference for the local radius measurement along the vessels. This radius is estimated on each Sa-CPR axial slice by pointing the upper north point of the vessel. Figure 5 shows a reconstruction of the vascular structure through a radial-variant tube centered on the corrected centreline.

3.2. Coronary arterial tree labelling

Figures 6-8 display several labeled slices (a) from the coronary artery MRA dataset #2. An approximate location of the slice plane is given on a schematic view of the heart (b). The arterial segments that can be seen on the slices are represented as sharp on the coronary artery map, the non visible vessels being blurred (c). Figure 2 illustrates the manual extraction of the coronary arteries from the ten datasets. The extracted segments are reported in tables 5 and 6. This analysis demonstrates the merits of MR imaging for coronary arteries. The whole proximal and medial segments have been extracted, and even the distal locations for the most part of the datasets. However, whereas these merits are obvious in the case of a global coronary anatomy exploration, we are interested in the following in assessing the MR

9

	Dataset									
	1	2	3	4	5	6	7	8	9	10
RCA(p)	E	E	E	E	E	E	E	E	E	E
RCA(m)	E	E	E	E	E	E	E	E	E	E
RCA(d)	E	E	E	E	E	E	E	E	E	E
RPD	E	E	E	.	E	E	E	.	E	.
RPA	E	E	E	E	E	E	E	.	E	E
RPL(1)	.	E	E	.	E	.	.	.	.	.
PDS	.	.	.	.	.	E	.	.	.	.
RCA-AM	.	E	.	.	.	.	.	E	.	E

Tab. 5: Summary of extracted RCA segments. E stands for "extracted".

modality for quantification purposes.

3.3. Quantitative analysis

The characteristics presented in this work are : (i) the length of each coronary arterial segments, as well as their estimated radii, according to the manually extracted and corrected centreline ; (ii) the image intensity probed along the corrected centreline.

3.3.1. Extracted length

Figure 9 shows the mean length of each coronary artery segment. No surprisingly, the proximal to medial segments have a length close to those reported in [25] when they exist. The relative error is due to the anatomical variations between subjects. For distal segments, no reliable comparison can be made due to the fact that they are far to be entirely extracted.

	Dataset									
	1	2	3	4	5	6	7	8	9	10
LM	E	E	E	E	E	E	E	E	E	E
LAD(p)	E	E	E	E	E	E	E	E	E	E
LAD(m)	.	E	E	E	E	E	E	E	E	E
LAD(d)	.	E	E	.	E	E	E	.	.	E
DIAG(1)	E	E	E	.	E	E	E	E	.	.
DIAG(2)	.	.	.	.	.	.	.	E	.	.
DIAG(3)	.	.	.	.	.	E	E	.	.	.
CX(p)	E	E	E	E	E	E	E	E	E	E
CX(md)	E	E	E	E	E	E	E	E	E	E
OBTM(1)	.	E	.	.	E	.	.	.	E	.
OBTM(2)	.	.	.	.	E	.	.	.	.	.

Tab. 6: Summary of extracted LCA segments. E stands for "extracted".

3.3.2. Estimated radii

As the radius is expected to decrease along a vessel, the result is presented through a simple linear regression. Figure 10 depicts the manually-pointed data and the corresponding regression line. The regression slope is negative $(-4.33E - 03)$, that confirms the general decreasing trend expected along a vessel. Results over the whole database and for each segment are summarized in table 7. The whole database presents a slowly-decreasing radius along the arterial segments, except for CX-2 and LAD-3. The difficulty to reliably point the vessel wall can explain this low quality radius estimation. Furthermore, the radius is highly varying along the vessels. The absolute Pearson correlation coefficient $|r|$ is adequatly lower than $\sqrt{3}/2$, meaning that the dispersion around the regression line prevents a correct radius prediction. The low MRA vessel contrast and the inherent difficulties to keep a 3D continuity through 2D manual analysis explain the observed errors.

3.3.3. Intensity measurement

An analysis of the intensity profiles along the coronary arteries has been performed. Figure 11 shows such a profile along the RCA of the volume #1. It can be observed that local variations are important. The simple regression line is also drawn on the chart. The results for each segment is displayed (slope a, y-intercept b, absolute correlation coefficient $|r|$ and mean) in table 8. Although the slope of the regression lines are closed to zero reflecting an almost-constant intensity at centreline, the correlation coefficients show in most cases significant variations.

Indeed, not only the intensity is highly-varying along the vessels but as the figure 12 shows, major differences appear between different datasets, with

	a	b	$\lvert r \rvert$	Mean (mm)
LM	-5.75e-2	2.08	0.44	1.76
DIAG(1)	-5.72e-3	1.37	0.41	1.11
LAD(p)	-4.07e-3	1.49	0.25	1.33
LAD(m)	-3.47e-4	1.1	0.01	1.14
LAD(d)	8.41e-4	1.23	0.01	1.23
CX(p)	-3.99e-3	1.36	0.27	1.22
CX(md)	1.94e-3	1.12	0.11	1.19
CX(g)	-1.82e-3	1.19	0.26	1.08
OBTM(1)	-2.07e-2	1.38	0.71	1.01
RCA(pmd)	-3.21e-3	1.78	0.3	1.58
RPD	-8.50e-3	1.23	0.32	1.1
RPA	-6.02e-3	1.31	0.32	1.14
RPL(1)	-3.91e-3	1.3	0.3	1.15

TAB. 7: Linear regression over local estimated radius along each segment. Regression line slope is a, y-intercept is b and Pearson coefficient is r.

	a	b	$|r|$	Mean
LM	5.65	323.78	0.2	354.66
DIAG(1)	-0.54	257.76	0.35	237.77
LAD(p)	-0.71	315.29	0.24	282.27
LAD(m)	-0.19	238.17	0.08	230.46
LAD(d)	-1.18	249.3	0.1	224.48
CX(p)	-0.99	341.01	0.28	305.21
CX(md)	-0.23	221.87	0.01	217.99
CX(g)	-0.5	205.94	0.48	177.11
OBTM(1)	-0.07	202.23	0.01	201.08
RCA	0.2	273.93	0.01	285.24
RPD	-1.48	281.3	0.3	253.57
RPA	-1.05	297.26	0.38	260.03
RPL(1)	-2.17	289.77	0.57	229.71

TAB. 8: Linear regression over intensity measurement along each segment. Regression line slope is a, y-intercept is b and Pearson coefficient is r.

mean intensities along the whole trees ranging from 186 to 469. It emphases the need for normalized intensities, such as it was proposed in [26].

3.4. Discussion

The qualitative analysis of coronary arterial tree extraction using whole-heart SSFP MRA points out that the main segments, up to distal parts, are unambiguously localized and labeled. Proximal diagonal segments have been also identified on seven of the 10 datasets. A number of marginal and septal segments were extracted.

This quantitative analysis that aimed to extract the lengths, local radii and local intensities along the arterial centrelines leads to mixed results. The extracted lengths confirm the qualitative analysis with figures closed to anatomical references and variabilities, but the local radius estimations and intensity measurements do not provide enough reliability for diagnosis or interventional planning.

Furthermore, the manual extraction of the coronary tree is highly time-consuming and is not applicable in clinical routine. A reliable estimation of the radius requires to point more than the only upper points of the vessel lumen.

These findings support the need for automatic or at least semi-automatic methods. They should avoid intra- and inter-operator biases and fasten the extraction process. The challenging points concern :

1. The low vessel spatial resolution : 4-voxels diameter for proximal main segment, down to 1-voxel diameter for distal segments
2. The high intensity variability along a vessel, making threshold-based method setting tedious

15

3. The high intensity inter-patient variability

4. the loss of signal due to either pathology or artifacts (motion, suscep-
   tibility,...)

5. The proximity of bright structures (veins, ventricles)

In the next section, we apply an existing semi-automatic method and compare the results with those obtained manually.

4. Preliminar testing of a semi-automatic segmentation method

4.1. State-of-the art methods

Most basic tools designed so far have been mainly applied to X-ray modalities and are based on intensity thresholding [27]. They are daily used as part of scanner marketed software packages including 3D volume rendering functionnalities. The vessel intensities being highly variable inside and along a vessel, thresholding can not be considered as reliable. Smarter segmentation methods are based on region growing (RG) [28]. For the same reasons of heterogeneity, a RG algorithm cannot extract the whole vascular tree without many expert interactions. Other methods rely on the tube-like structure as a prior knowledge. A joint fast-marching/level set method is proposed in [29] which offers the capability to build a vascular tree thanks to a minimal path technique. In [30], 3D geometrical moments were used to get the center and the principal axis of a vessel that feeds a spatial tracking algorithm. Geometrical moments and level-set methods have been combined in [31]. An artificial life-based method is also reported in [32] and a mathematical morphology approach is described in [33]. One can refer to [34] for a review on vessel extraction methods.

Although these segmentation methods show promising results, they have been mainly tested on X-Ray angiography or MDCT modalities. In the following, we assess a modified geometrical moment-based tracking method integrating multiple hypothesis testing and regularization (MH-GMT) [35] and we compare its performance to the manual extraction carried out above, considered here as ground truth.

4.2. Extraction results

Briefly speaking (more algorithmic details can be found in [35]), the geometrical moment-based tracking methods are designed to extract a $3D$ curve from a volume, following a particular feature. As geometrical moment are able to compute the local orientation of a cylinder from image intensities, it is well-suited for vessel centreline extraction. The tracking starts from a seed point and iteratively builds a curve from the estimated orientations until a stopping criterion is reached. The idea behind the multiple hypotheses framework is to automatically browse the parameters of the algorithm (eg. moment kernel size, stopping criterion,...) to extract multiple centrelines and then select the best one.

The bunch of candidate centrelines is shown figure 13 for the 10 arterial trees together with the seed point locations. Each centreline is the output of the algorithm for one state of the parameter set.

4.3. Distance definition for quality measurement

In the following, we use the concepts of overdetection and underdetection to assess the quality of the extracted arterial tree. Let $\mathcal{T}_S$ be the tree obtained from MH-GMT and $\mathcal{T}_R$ the manually extracted one. If p is a point from $\mathcal{T}_S$

and q a point from $\mathcal{T}_R$, we define the overdetection distance as :

$$\forall p \in \mathcal{T}_S, OD_p = \min_{q \in \mathcal{T}_R} (||pq||) \tag{1}$$

This measure allows detecting points that belong to the semi-automatically extracted tree $\mathcal{T}_S$ but do not belong to the reference tree. Figure 14(a) shows the overdetection distance (OD) for each point and the histogram in figure 14(c) points out that the majority of the points are less than $2mm$ far from the reference. Only 3% of points may correspond to false positive detections.

The symmetric measure of (1) is the underdetection distance, able to detect vessels from $\mathcal{T}_R$ that cannot be find in $\mathcal{T}_S$ and defined as :

$$\forall q \in \mathcal{T}_R, UD_q = \min_{p \in \mathcal{T}_S} (||pq||) \tag{2}$$

The visualization of UD for each reference point (figure 14(b) underlines the missing segments in $\mathcal{T}_S$. However, the histogram (figure 14(d)) shows that 77% of the points from $\mathcal{T}_R$ are less than $2mm$ far from $\mathcal{T}_S$. 15% of points are farther than $5mm$, which may be lowered by adding few seed points. These results are summarized in table 9 for each dataset, where over- and underdetection are presented as the number of points with OD and UD less than $2mm$ in percent. The rates of correspondance are relatively high between the semi-automatic extraction and the ground truth. It can be seen that the number of seed points remains reasonable with respect to the interaction time required to the user. The computation time is also compatible with the clinical constraints.

	Number of seed points	Time (s)	OD % < 2mm	OD % > 5mm	UD % < 2mm	UD % > 5mm
1	7	8	0.91	0.04	0.81	0.10
2	11	19	0.97	0.00	0.76	0.16
3	10	9	0.91	0.03	0.88	0.06
4	6	9	0.81	0.07	0.66	0.20
5	10	14	0.89	0.03	0.71	0.20
6	8	15	0.94	0.02	0.82	0.11
7	8	10	0.90	0.02	0.63	0.25
8	5	7	0.87	0.8	0.77	0.19
9	6	9	0.95	0.00	0.96	0.00
10	3	6	0.92	0.03	0.70	0.25
Mean	7	10.6	0.90	0.03	0.77	0.15

TAB. 9: Summary of the semi-automatic coronary artery centreline extraction.

5. Conclusion

Cardiac imaging is now able to provide 3D static data sets but also 3D image sequences and open new perspectives for diagnosis and image guided interventions. In this context, MR imaging is very attractive and has been widely investigated for coronary vessel analysis. With SSFP MR sequence, a whole heart volume can be acquired in a free breath fashion in less than 15 minutes, thus improving the patients comfort.

We have shown that an unambiguous labeling of large parts of coronary arteries can be achieved. To our knowledge, such a proof of the potential of MR imaging for coronary analysis is lacking at this depth. A global coronary anatomy can thus be reconstructed, bringing useful information for interventional planning. However, the coronary tree is built from many points

manually placed in the volume, requiring too much interaction and time for a clinical use.

A semi-automatic extraction method has therefore been applied. It is based on geometrical moments and outputs the central axes of the vessels. Results are promising as the labeled vessels are retrieved thanks to only 13 seed points on average. Therefore, for qualitative applications on coronary anatomy, MR leads to a performance comparable to MDCT [36] without using any contrast product.

Improvements however are necessary. They will come first from the MR imaging (new acquisition sequences, contrast agents, etc.) where continuous advances are observed. They will also come from advances of detection and segmentation algorithms with lower time computation, higher robustness and reduced interaction. The quantification of patient-specific coronary features is required to reach a better diagnosis and to help in planning the interventions such as CRT as far as the the coronary sinus and the whole left venous tree is also extracted. The competition between imaging modalities and especially MDCT and MRA is a factor of progress that will help in such objectives.

6. Acknowledgements

7. References

Références

[1] D. Lloyd-Jones, R. Adams, M. Carnethon, G. D. Simone, T. B. Ferguson, K. Flegal, E. Ford, K. Furie, A. Go, K. Greenlund, N. Haase, S. Hailpern, M. Ho, V. Howard, B. Kissela, S. Kittner, D. Lackland, L. Lisabeth, A. Marelli, M. McDermott, J. Meigs, D. Mozaffarian, G. Nichol, C. O'Donnell, V. Roger, W. Rosamond, R. Sacco, P. Sorlie, R. Stafford, J. Steinberger, T. Thom, S. Wasserthiel-Smoller, N. Wong, J. Wylie-Rosett, Y. Hong, A. H. A. S. Committee, S. S. Subcommittee, Heart disease and stroke statistics – 2009 update : a report from the American Heart Association Statistics Committee and Stroke Statistics Subcommittee., Circulation 119 (3) (2009) 480–486.

[2] X. Bi, D. Li, Coronary arteries at 3.0 T : Contrast-enhanced magnetization-prepared three-dimensional breathhold MR angiography., J Magn Reson Imaging 21 (2) (2005) 133–139.

[3] F. Renard, Y. Yang, Coronary artery extraction and analysis for detection of soft plaques in MDCT images, in : Proc. 15th IEEE International Conference on Image Processing ICIP 2008, 2008, pp. 2248–2251.

[4] J. C. Daubert, C. Leclercq, E. Donal, P. Mabo, Cardiac resynchronisation therapy in heart failure : Current status, Heart Fail Rev 11 (2) (2006) 147–154.

[5] K. Rioual, E. Unanua, S. Laguitton, M. Garreau, D. Boulmier, P. Haigron, C. Leclercq, J.-L. Coatrieux, MSCT labelling for pre-operative

planning in cardiac resynchronization therapy, Comput Med Imaging Graph 29 (6) (2005) 431–439.

[6] J. T. Dodge, B. G. Brown, E. L. Bolson, H. T. Dodge, Intrathoracic spatial location of specified coronary segments on the normal human heart. Applications in quantitative arteriography, assessment of regional risk and contraction, and anatomic display., Circulation 78 (5 Pt 1) (1988) 1167–1180.

[7] J. T. Dodge, B. G. Brown, E. L. Bolson, H. T. Dodge, Lumen diameter of normal human coronary arteries. Influence of age, sex, anatomic variation, and left ventricular hypertrophy or dilation., Circulation 86 (1) (1992) 232–246.

[8] C. Chalopin, G. Finet, I. E. Magnin, Modeling the 3D coronary tree for labeling purposes., Med Image Anal 5 (4) (2001) 301–315.

[9] M. Garreau, J. L. Coatrieux, R. Collorec, C. Chardenon, A knowledge-based approach for 3-D reconstruction and labeling of vascular networks from biplane angiographic projections., IEEE Trans Med Imaging 10 (2) (1991) 122–131.

[10] C. Lorenz, J. von Berg, A comprehensive shape model of the heart., Med Image Anal 10 (4) (2006) 657–670.

[11] A. Bousse, J. Zhou, G. Yang, J.-J. Bellanger, C. Toumoulin, Motion Compensated Tomography Reconstruction of Coronary Arteries in Rotational Angiography 56 (4) (2009) 1254–1257.

[12] J. Zhou, A. Bousse, G. Yang, J.-J. Bellanger, L. Luo, C. Toumoulin, J.-L. Coatrieux, A blob-based tomographic reconstruction of 3D coronary trees from rotational x-ray angiography, Vol. 6913, SPIE, 2008, p. 69132N.

[13] G. Schoonenberg, A. Neubauer, M. Grass, Three-Dimensional Coronary Visualization, Part 2 : 3D Reconstruction, Cardiology Clinics 27 (3) (2009) 453 – 465.

[14] N. R. V. de Veire, J. D. Schuijf, G. B. Bleeker, M. J. Schalij, J. J. Bax, Magnetic resonance imaging and computed tomography in assessing cardiac veins and scar tissue., Europace 10 Suppl 3 (2008) 110–113.

[15] W. Y. Kim, P. G. Danias, M. Stuber, S. D. Flamm, S. Plein, E. Nagel, S. E. Langerak, O. M. Weber, E. M. Pedersen, M. Schmidt, R. M. Botnar, W. J. Manning, Coronary magnetic resonance angiography for the detection of coronary stenoses., N Engl J Med 345 (26) (2001) 1863–1869.

[16] M. Stuber, R. G. Weiss, Coronary magnetic resonance angiography., J Magn Reson Imaging 26 (2) (2007) 219–234.

[17] H. Sakuma, Y. Ichikawa, N. Suzawa, T. Hirano, K. Makino, N. Koyama, M. V. Cauteren, K. Takeda, Assessment of coronary arteries with total study time of less than 30 minutes by using whole-heart coronary MR angiography., Radiology 237 (1) (2005) 316–321.

[18] B. Giorgi, S. Dymarkowski, F. Maes, M. Kouwenhoven, J. Bogaert, Improved Visualization of Coronary Arteries Using a New Three-

Dimensional Submillimeter MR Coronary Angiography Sequence with Balanced Gradients, Am. J. Roentgenol. 179 (4) (2002) 901–910.

[19] M. Ozgun, A. Hoffmeier, M. Kouwenhoven, R. M. Botnar, M. Stuber, H. H. Scheld, W. J. Manning, W. Heindel, D. Maintz, Comparison of 3D Segmented Gradient-Echo and Steady-State Free Precession Coronary MRI Sequences in Patients with Coronary Artery Disease, Am. J. Roentgenol. 185 (1) (2005) 103–109.

[20] P. G. Danias, A. Roussakis, J. P. A. Ioannidis, Diagnostic performance of coronary magnetic resonance angiography as compared against conventional X-ray angiography : a meta-analysis., J Am Coll Cardiol 44 (9) (2004) 1867–1876.

[21] P. Beerbaum, S. Sarikouch, K.-T. Laser, G. Greil, W. Burchert, H. Krperich, Coronary anomalies assessed by whole-heart isotropic 3D magnetic resonance imaging for cardiac morphology in congenital heart disease., J Magn Reson Imaging 29 (2) (2009) 320–327.

[22] P. J. Scanlon, D. P. Faxon, A. M. Audet, B. Carabello, G. J. Dehmer, K. A. Eagle, R. D. Legako, D. F. Leon, J. A. Murray, S. E. Nissen, C. J. Pepine, R. M. Watson, J. L. Ritchie, R. J. Gibbons, M. D. Cheitlin, T. J. Gardner, A. Garson, R. O. Russell, T. J. Ryan, S. C. Smith, ACC/AHA guidelines for coronary angiography. A report of the American College of Cardiology/American Heart Association Task Force on practice guidelines (Committee on Coronary Angiography). Developed in collaboration with the Society for Cardiac Angiography and Interventions., J Am Coll Cardiol.

[23] A. Kanitsar, D. Fleischmann, R. Wegenkittl, P. Felkel, E. Groller, CPR - curved planar reformation, in : Proc. IEEE Visualization VIS 2002, 2002, pp. 37–44.

[24] M. Schaap, C. T. Metz, T. van Walsum, A. G. van der Giessen, A. C. Weustink, N. R. Mollet, C. Bauer, H. Bogunovi, C. Castro, X. Deng, E. Dikici, T. O'Donnell, M. Frenay, O. Friman, M. H. Hoyos, P. H. Kitslaar, K. Krissian, C. Khnel, M. A. Luengo-Oroz, M. Orkisz, O. Smedby, M. Styner, A. Szymczak, H. Tek, C. Wang, S. K. Warfield, S. Zambal, Y. Zhang, G. P. Krestin, W. J. Niessen, Standardized evaluation methodology and reference database for evaluating coronary artery centerline extraction algorithms., Med Image Anal 13 (5) (2009) 701–714.

[25] C. Christids, C. Cabrol, Anatomie des artères coronaires du coeur, J. B. Bailliere, 1976.

[26] O. M. Weber, S. Pujadas, A. J. Martin, C. B. Higgins, Free-breathing, three-dimensional coronary artery magnetic resonance angiography : comparison of sequences., J Magn Reson Imaging 20 (3) (2004) 395–402.

[27] U. J. Schoepf, CT of the heart : principles and applications, Humana Press, Totowa, N.J, 2005.

[28] T. Boskamp, D. Rinck, F. Link, B. Kmmerlen, G. Stamm, P. Mildenberger, New vessel analysis tool for morphometric quantification and visualization of vessels in CT and MR imaging data sets., Radiographics 24 (1) (2004) 287–297.

[29] L. D. Cohen, T. Deschamps, Segmentation of 3D tubular objects with adaptive front propagation and minimal tree extraction for 3D medical imaging, Comput Methods Biomech Biomed Engin 10 (4) (2007) 289–305.

[30] C. Boldak, C. Toumoulin, J. L. Coatrieux, 3D segmentation and characterization of lower limb vessels in multi-slice computed tomography, in : Proc. 25th Annual International Conference of the IEEE Engineering in Medicine and Biology Society, Vol. 1, 2003, pp. 580–583 Vol.1.

[31] A. Bousse, C. Boldak, C. Toumoulin, G. Yang, S. Laguitton, D. Boulmier, Coronary extraction and characterization in multi-detector computed tomography, ITBM-RBM 27 (5-6) (2006) 217 – 226.

[32] C. McIntosh, G. Hamarneh, Vessel Crawlers : 3D Physically-based Deformable Organisms for Vasculature Segmentation and Analysis, in : Proc. IEEE Computer Society Conference on Computer Vision and Pattern Recognition, Vol. 1, 2006, pp. 1084–1091.

[33] B. Bouraoui, C. Ronse, J. Baruthio, N. Passat, P. Germain, Fully automatic 3D segmentation of coronary arteries based on mathematical morphology, in : Proc. 5th IEEE International Symposium on Biomedical Imaging : From Nano to Macro ISBI 2008, 2008, pp. 1059–1062.

[34] D. Lesage, E. D. Angelini, I. Bloch, G. Funka-Lea, A review of 3D vessel lumen segmentation techniques : Models, features and extraction schemes., Med Image Anal.

[35] J. Velut, C. Toumoulin, J.-L. Coatrieux, 3D coronary structure tracking algorithm with regularization and multiple hypotheses in MRI, in : ISBI, 2010, pp. 37–40.

[36] A. Larralde, C. Boldak, M. Garreau, C. Toumoulin, D. Boulmier, Y. Rolland, Evaluation of a 3D Segmentation Software for the Coronary Characterization in Multi-slice Computed Tomography, in : Functional Imaging and Modeling of the Heart, 2003, pp. 39–51.

Conflit d'intérêt : aucun
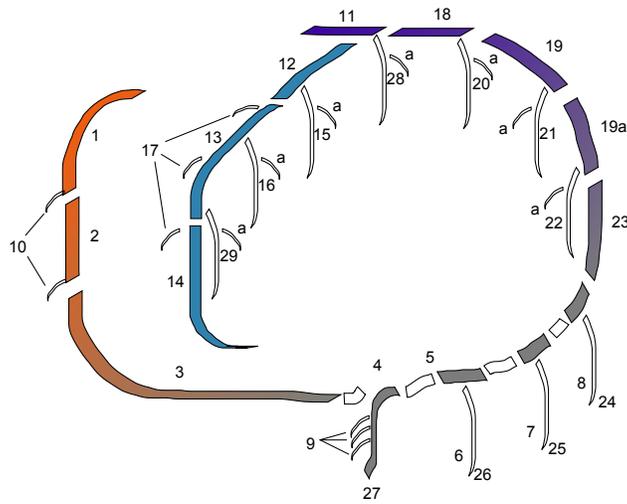
FIG. 1: Coronary artery map as proposed by the AHA [22]. A correspondance between figures and segment names is given in tables 3 and 4.

(a) Dataset #1   (b) Dataset #2   (c) Dataset #3

(d) Dataset #4   (e) Dataset #5   (f) Dataset #6

(g) Dataset #7   (h) Dataset #8   (i) Dataset #9

(j) Dataset #10
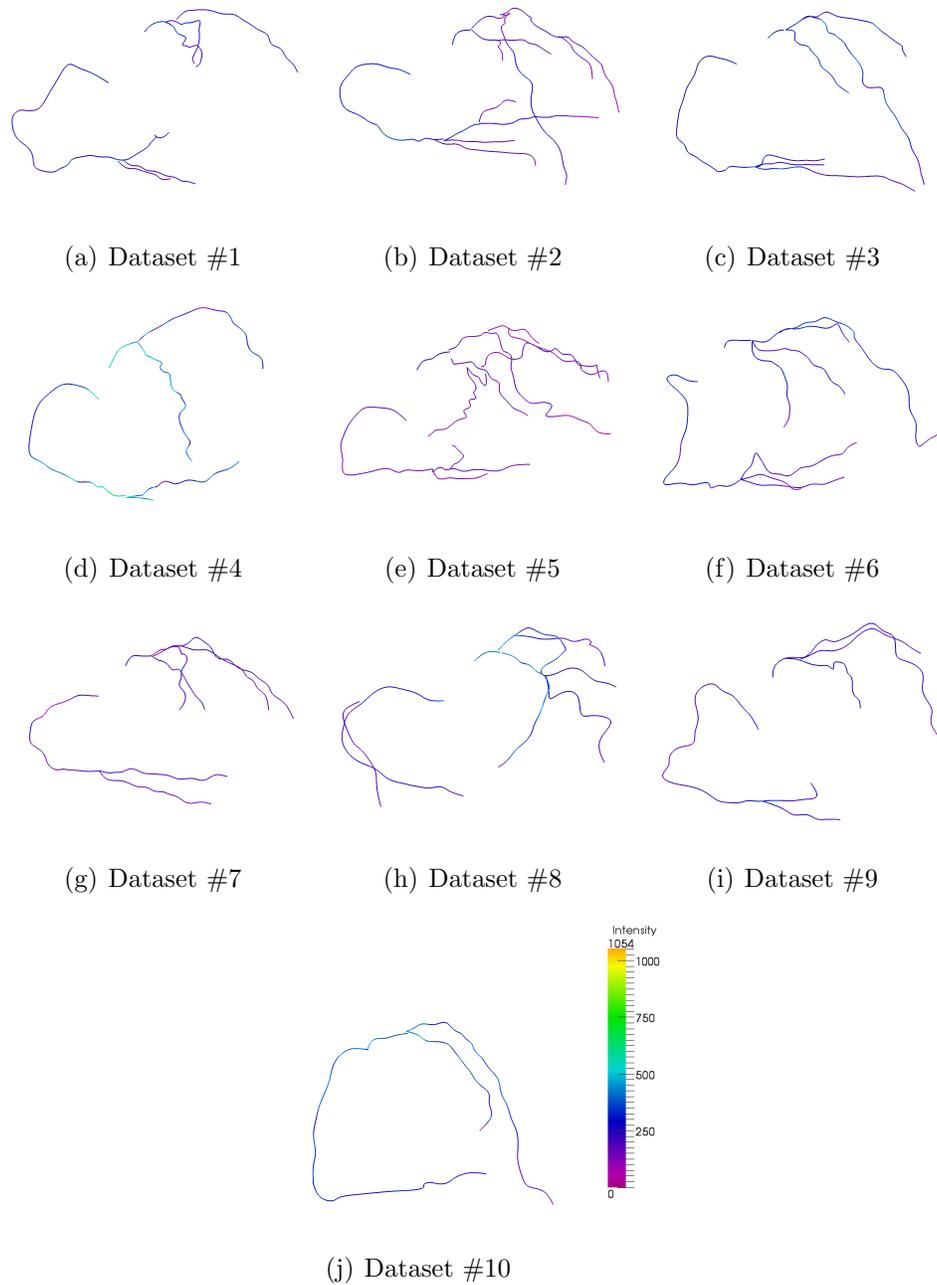
FIG. 2: Coronal views of ten coronary arterial trees manually extracted from MRA and the image intensity probed along the vessels.

30
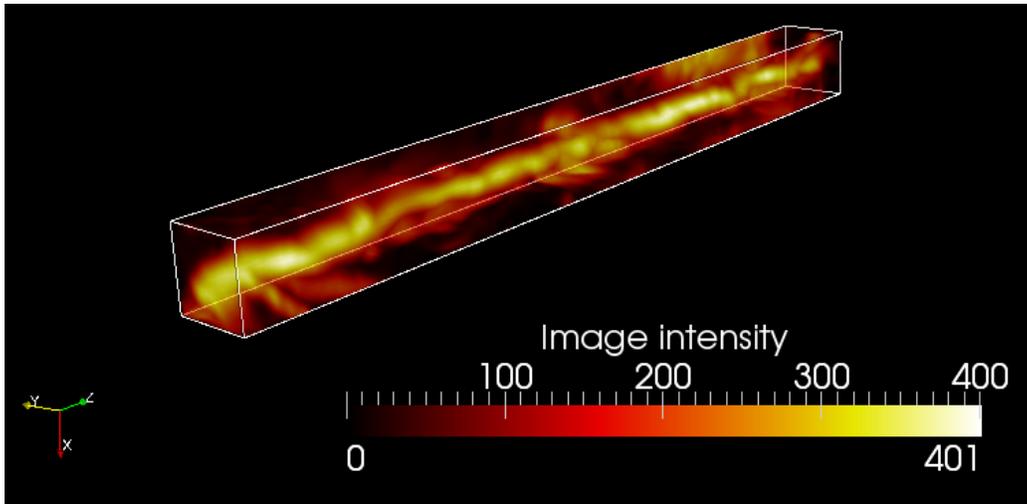
FIG. 3: Straightened Curved Planar Reformation of the 1st, 2nd and 3rd RCA segments. MIP (Maximum Intensity Projection) visualisation.
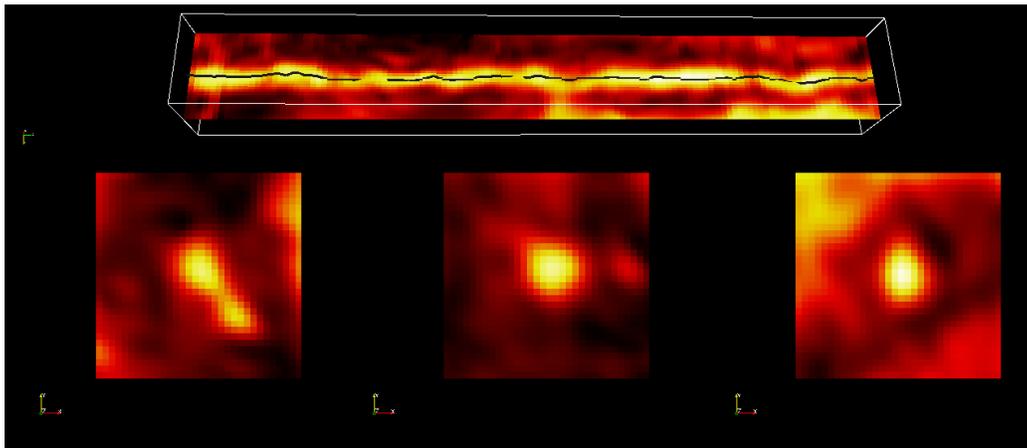
FIG. 4: Centreline correction process. Corrected vessel centres are pointed slice by slice.
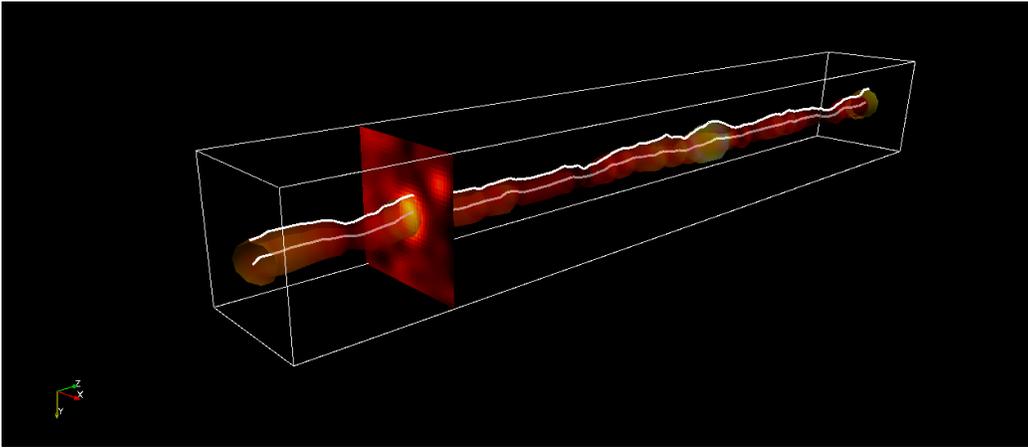
Fig. 5: Sa-CPR reconstruction of the vascular wall (1st, 2nd and 3rd segments).
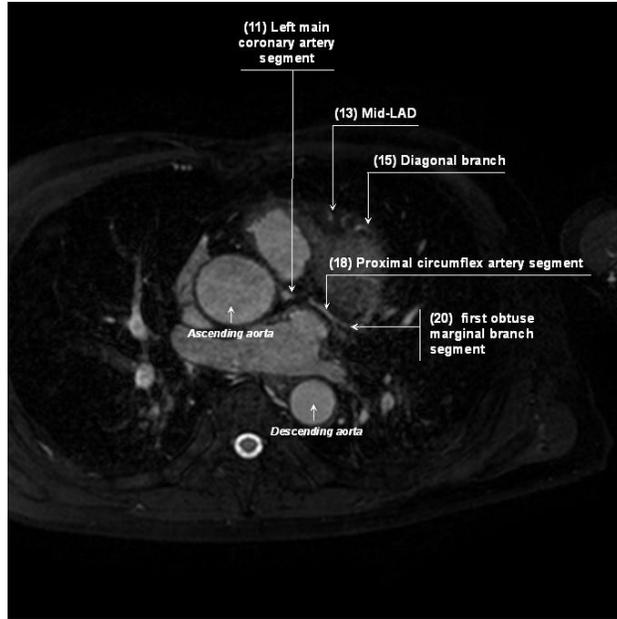
(a) Labels
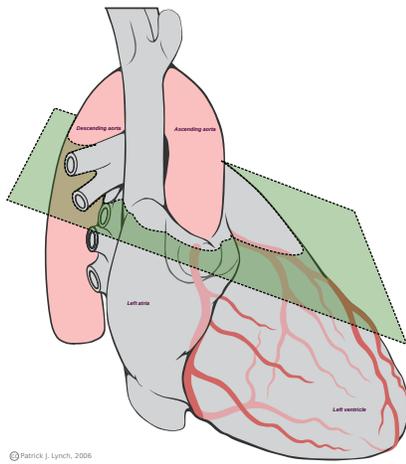
(b) Approximate slice position
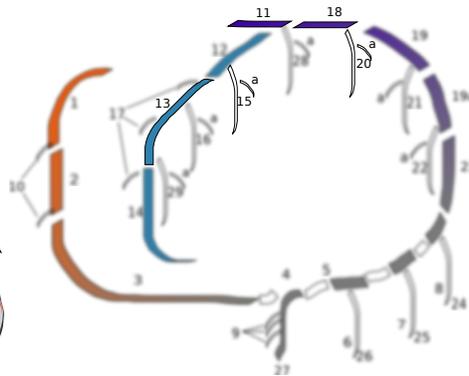
(c) Visible segments

Fig. 6: Proximal left coronary artery
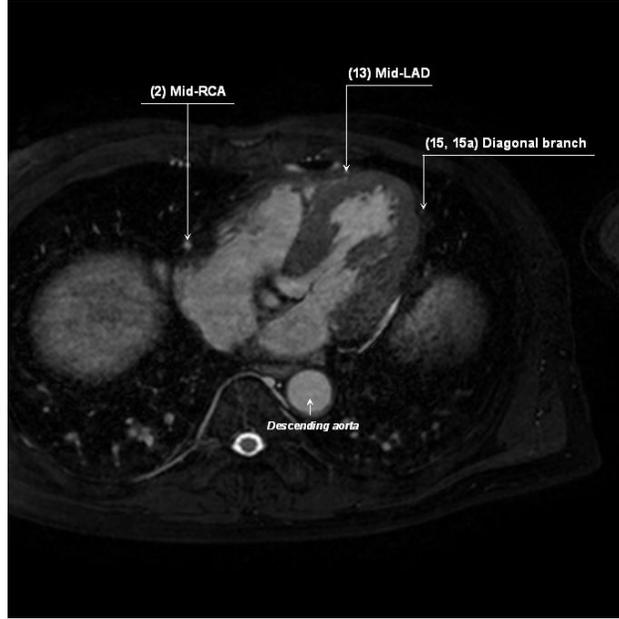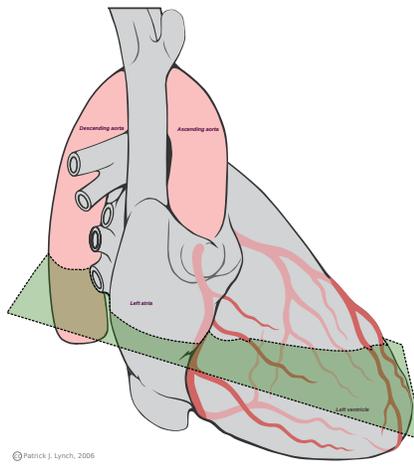
(a) Labels

(b) Approximate slice position
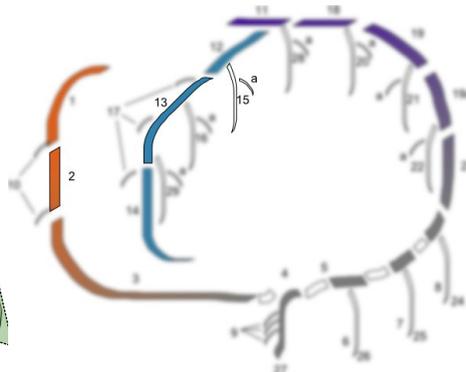
(c) Visible segments

FIG. 7: Mid-distal right coronary artery
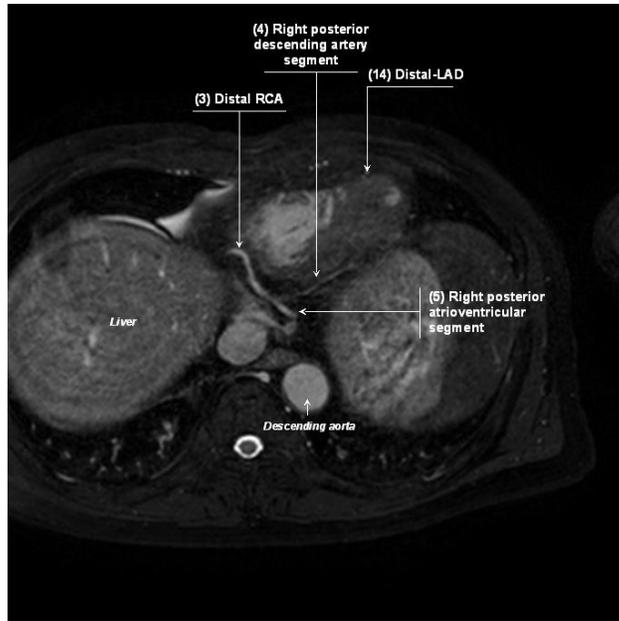
(a) Labels
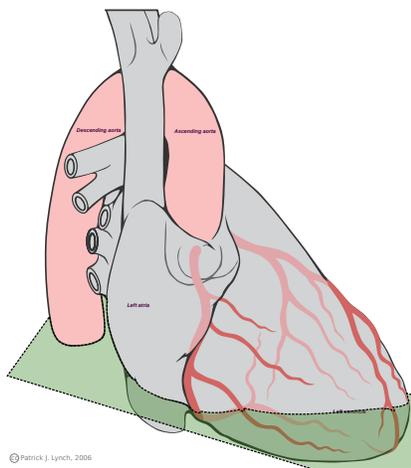
(b) Approximate slice position
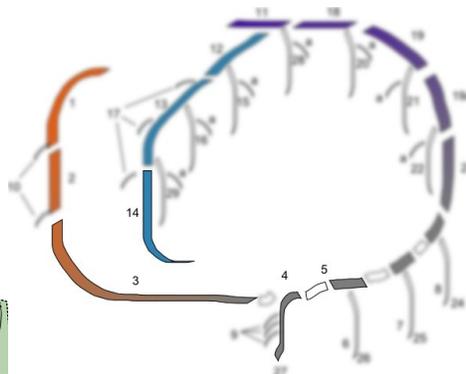
(c) Visible segments

FIG. 8: Distal right coronary artery, right posterior segments and distal left coronary artery
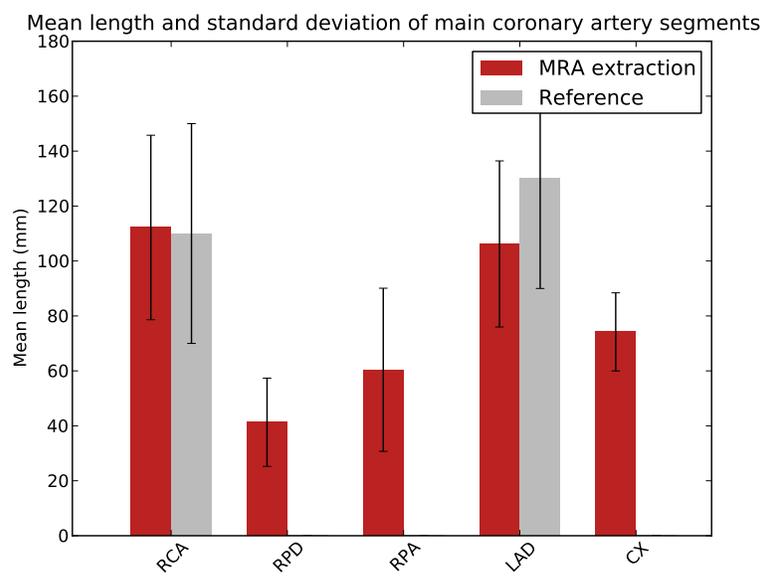
Fig. 9: Mean lengths of extracted arterial segments over the ten MRA datasets
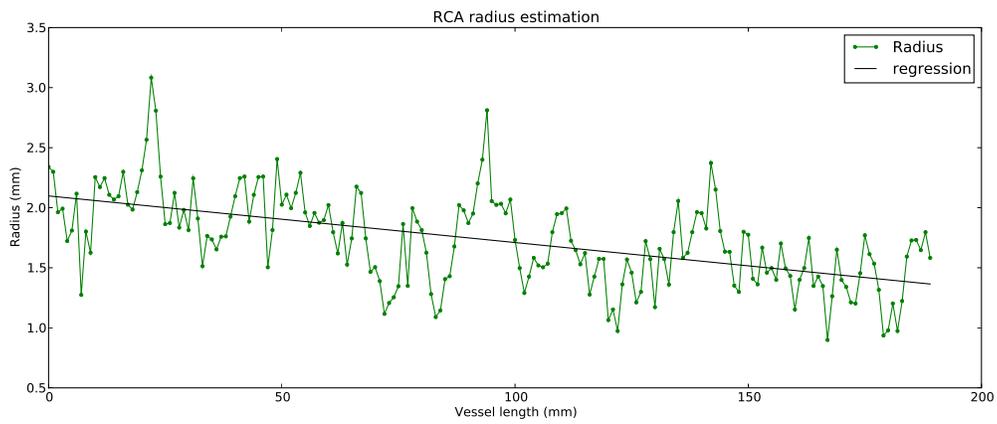
Fɪɢ. 10: Radius estimation along the RCA(p), RCA(m) and RCA(d)segments
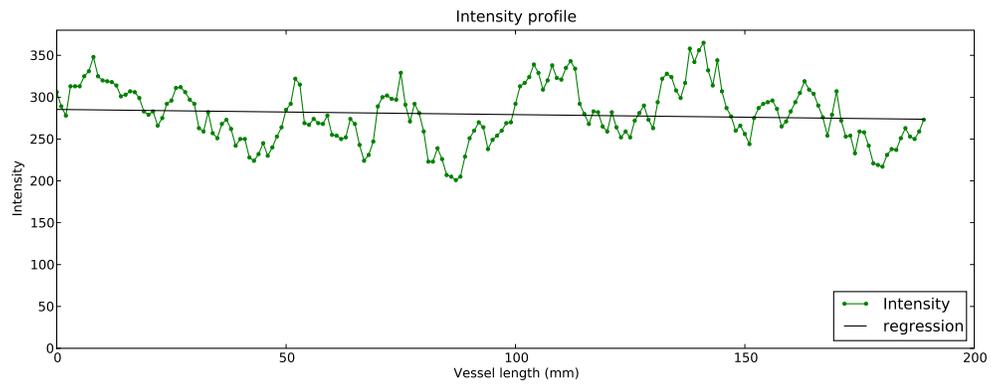
Fɪɢ. 11: Intensity measurement along the RCA(p), RCA(m) and RCA(d) segment centre-lines
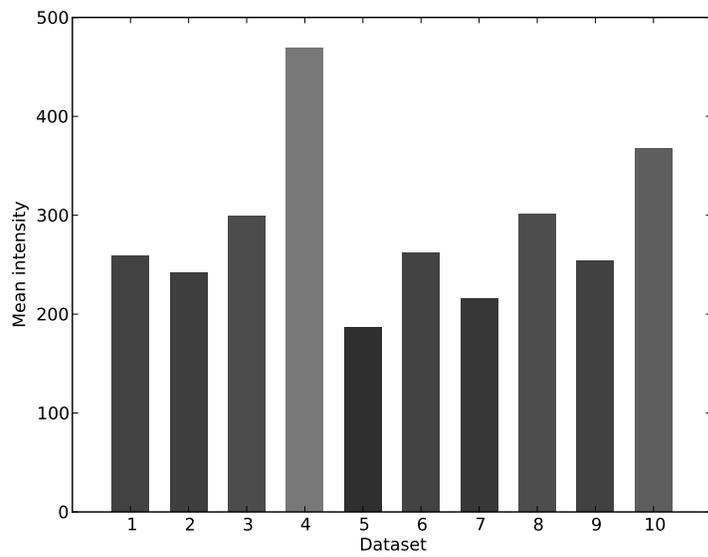
FIG. 12: Mean intensity along the coronary artery centreline for each dataset. Bars are gray-colored according to the intensity.
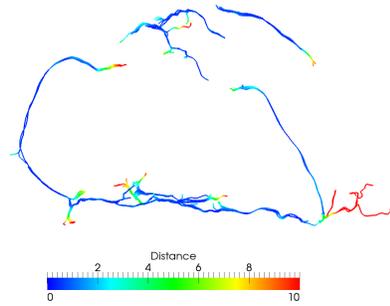
(a) Dataset #1

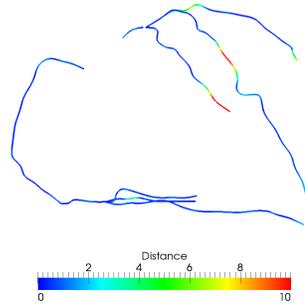(b) Dataset #2

(c) Dataset #3

(d) Dataset #4

(e) Dataset #5

(f) Dataset #6

(g) Dataset #7
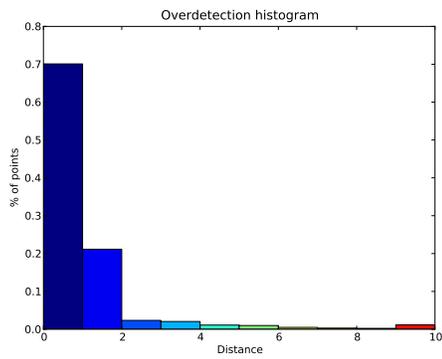
(h) Dataset #8

(i) Dataset #9

(j) Dataset #10
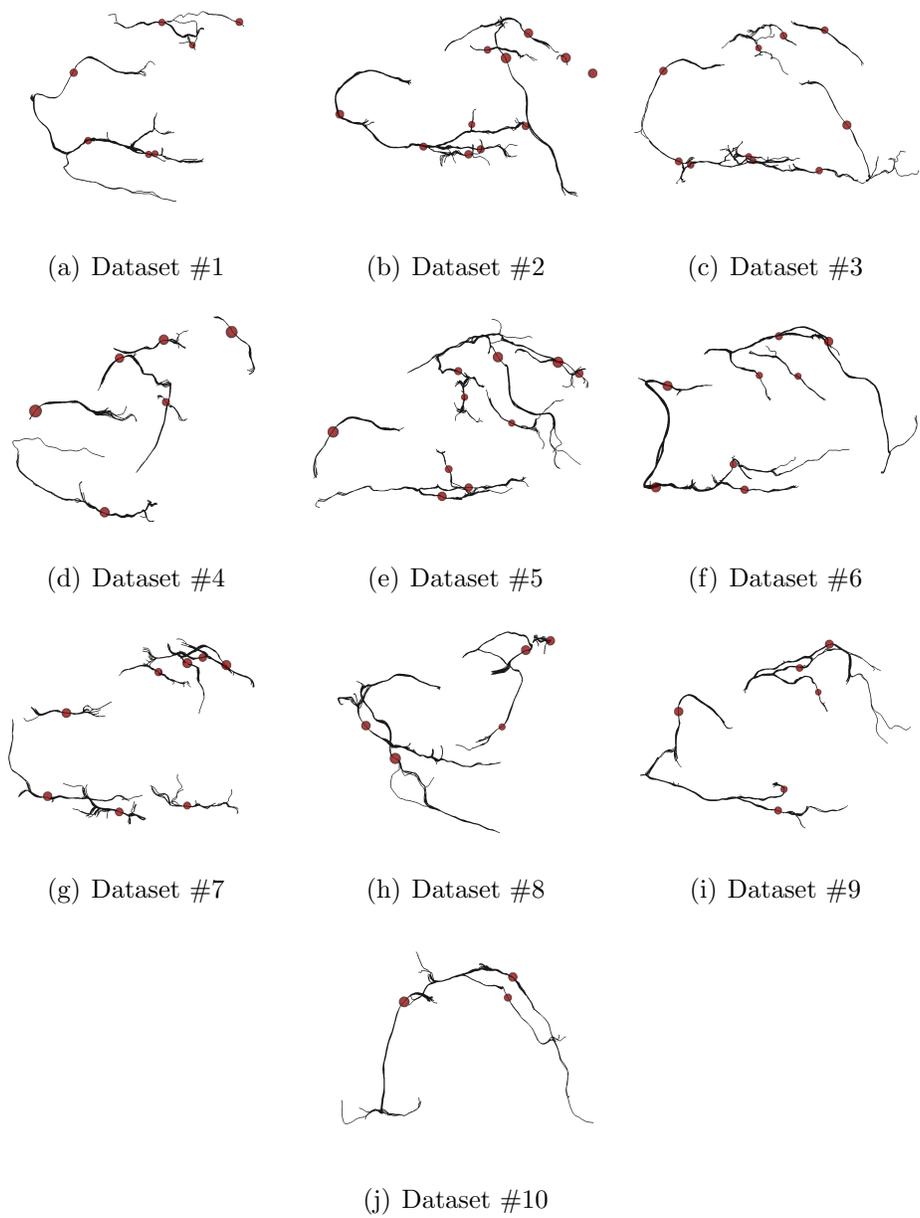
FIG. 13: Coronal view of the ten arterial tree obtained with MH-GMT method. Red spheres depict the seed points locations.
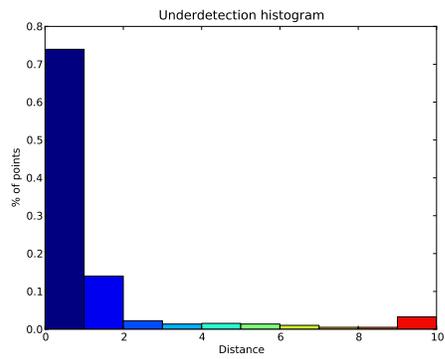
(a) Overdetection

(b) Underdetection

(c) Histogram of OD distances

(d) Histogram of UD distances

FIG. 14: A quality assessment through over- and under-detection. The last bin in the histograms cumulates the number of points with distance greater or equal than $9mm$.